Estimation of the Marine Boundary Layer Height over the Central North Pacific Using GPS Radio Occultation

Thomas E. Winning Jr.*[1,2], Yi-Leng Chen[1], Feiqin Xie[2]

[1]Department of Atmospheric Science, School of Ocean and Earth Science and Technology, University of Hawai'i - Mānoa, 2525 Correa Rd, HIG 342, Honolulu, HI 96822 USA

(808) 956-2570 – yileng@hawaii.edu

[2]Department of Physical and Environmental Sciences, College of Science and Engineering, Texas A&M University Corpus Christi, 6300 Ocean Dr., Unit 5850, Corpus Christi, TX 78412 USA

(361) 825-5850 – Feiqin.Xie@tamucc.edu

*Corresponding author: Thomas E. Winning Jr.
Department of Physical and Environmental Sciences, College of Science and Engineering, Texas A&M University Corpus Christi, 6300 Ocean Dr., Unit 5850, Corpus Christi, TX, 78412
E-mail address: twinning@islander.tamucc.edu

Abstract

Global positioning system radio occultation (GPS RO) refractivity data obtained from the first Constellation Observing System for Meteorology, Ionosphere, and Climate (COSMIC) for the years 2007 to 2012 were used to estimate an overall climatology for the height of the marine boundary layer (MBL) over the central North Pacific Ocean including the Hawaiian Island region (10°N-45°N; 125°W-175°W). The trade wind days are identified based on the six-year National Centers for Environmental Prediction (NCEP) global analysis for the same period. About 87% of the RO soundings in summer (June-July-August, JJA) and 47% in winter (December-January-February, DJF) are under trade wind conditions. The MBL height climatology under trade wind conditions is derived and compared to the overall climatology. In general, MBL heights are lowest adjacent to the southern coast of California and gradually increase to the south and west. During the summer (JJA) when the northeasterly trade winds are the dominant surface flow, the median MBL height decreases from 2.0 km over Kauai to 1.9 km over the Big Island with an approximate 2 km maximum that progresses from southwest to northeast throughout the year. If the surface flow is restricted to trade winds only, the maximum MBL heights are located over the same areas, but they increase to a median height of 1.8 km during DJF and 2.1 km during JJA. For the first time, the GPS RO technique allows the depiction of the spatial variations of the MBL height climatology over the central North Pacific.

Keywords: Boundary layer, boundary layer height, trade wind, COSMIC, GPS Radio Occultation, Hawaii, refractivity

1. Introduction

The northeasterly surface flow over the central North Pacific Ocean is a manifestation of the North Pacific sub-Tropical High (NPSTH). The resulting low level flow, referred to as the trade winds (TW), represent the world's most consistent surface wind field (Malkus, 1956). Along its trajectory, subsiding air from upper levels comes into contact with convectively driven maritime air ascending from the surface. The transition layer between the two represents the interface between the marine boundary layer (MBL) and the subsiding warm and dry air aloft (Riehl, 1979). The air within MBL is characterized as moist, conditionally unstable, and frequently populated with trade wind cumuli. The subsidence warming in the inversion layer is balanced by radiative cooling and evaporation from the tops of trade cumuli (Riehl 1979; Albrecht et al., 1979; Betts and Ridgway, 1989). The transition layer is marked by a dramatic decrease in water vapor with respect to height and sometimes accompanied by an increase in temperature, which is referred to as the trade wind inversion (TWI). The inversion base varies from about 500 m at the eastern extreme of the subtropical high to about 2000 m at the western and equatorial extremities (Neiburger et al., 1961; Malkus and Riehl, 1964). The thickness of the transition layer, on average, is about 400-600 m; however, it can vary widely from a few tens of meters to almost 1 km (Bingaman, 2005). The influence of the MBL is expansive and is an instrumental component of stability and the vertical extent of the convective process, vertical heat and moisture fluxes, large-scale circulations, and energy transports (Trenberth and Stepaniak, 2003).

Over the Hawaiian Islands, the trade wind flow and TWI have significant impacts on island-scale airflow as well as local weather and climate. For islands with tops above the inversion, the TWI base serves as a lid forcing the incoming low-level trade wind flow to be deflected on the windward side (Leopold, 1949). Using model sensitivity tests Chen and Feng (2001) proved that airflow around the island is affected by the TWI and not by the upstream Froude number ($Fr = U/Nh$, where U is the cross mountain wind speed, N is stability, and h is the mountain height) alone (Smolarkiewicz et al., 1988; Rasmussen et al., 1989). For mountains with tops or ridges above the base of the TWI, areas of maximum rainfall correspond to regions of persistent orographic lifting of moisture-laden northeast trade winds up the windward slopes. Conversely, areas of low rainfall are found in the leeward areas and atop the highest mountains

(Giambelluca et al., 2013) and result in a semi-arid local climate (Giambelluca and Nullet, 1991; Chen and Nash, 1994; Chen and Wang, 1994). For islands with mountaintops or ridges below the TWI base, a rainfall maximum occurs at the summits (Giambelluca et al., 2013; Nguyen et al., 2010).

The height and strength of the TWI vary on a daily basis (Neiburger et al., 1961; Chen and Feng, 1995). The presence of the TWI limits the vertical extent of convective processes like cloud development. The short term variations of the TWI affect the day to day local weather over the Hawaiian Islands. Chen and Feng (1995) examined rainfall patterns over the Island of Hawaii (Big Island) under high and low trade wind inversions during the Hawaiian Rainband Project (HaRP). Their results suggest that for the low- (high-) inversion days, the median daily rainfall on the windward side of the Big Island is about one-half (more than twice) of the HaRP median daily rainfall. On high inversion days, the afternoon orographically induced clouds and showers extend closer to the summits than during low inversion days because the afternoon upslope flow can bring the low-level moist air to higher elevations. Chen and Feng (2001) simulated island airflow and weather for the Big Island under summer trade wind conditions. They showed that the TWI height represents the depth of the moist layer that affects cloud development and convective feedback to the island airflow. For islands with tops below the trade wind inversion, the daily rainfall amounts on the windward side and the mountaintops are higher when the inversion is higher (Hartley and Chen, 2010).

Despite its significant impacts on local weather and climate, except two sounding sites (Hilo and Lihue) (Fig. 1), information on the trade wind inversion over the central North Pacific is very limited. Soundings from these two stations are strongly affected by the terrain and local winds and may not be representative of the open ocean conditions. Throughout the year, radiosonde analysis reveals the MBL height on the windward side of the southeastern island of Hawaii (Fig. 1) is more than 200 m higher than at Lihue, which is located on the windward side of the northwestern island of Kauai (Tran, 1995; Bingaman, 2005; Cao et al., 2007). However, because the Island of Hawaii has massive volcanic cones with heights exceeding 4000 m, the differences in MBL height between Hilo and Lihue may not represent the actual spatial variations over the region (Garrett, 1980). Over the open ocean, the satellite derived temperature and moisture profiles do not have adequate resolution to depict the TWI layer. The launch of the first Constellation Observing System for Meteorology, Ionosphere, and Climate

(COSMIC) in 2006, allows for atmospheric profiling with 100 m vertical resolution to be extended over the open ocean using the GPS radio occultation (GPS RO) technique.

Previous research demonstrated the effectiveness of using the refractivity gradient method to detect the boundary layer height in the presence of a moisture gradient and temperature inversion (e.g., Basha and Rantam, 2009; Guo et al., 2011; Ao et al., 2012; Xie et al., 2012; Ho et al., 2015). Additionally, Zhou and Chen (2014) assimilated the high vertical resolution GPS RO data from COSMIC satellites into the initial conditions of the Weather Research and Forecasting (WRF) model. They showed that the TWI is better predicted for a summer trade wind case when GPS RO data is assimilated into the regional WRF models. Additionally, for a winter cold front case, the propagation of the cold front, prefrontal moisture tongue, and postfrontal inversion are better predicted in the high resolution regional domain over the Hawaiian Islands.

Using the data collected by COSMIC GPS RO, an analysis focusing on seasonal spatial variations of MBL height and strength over the Hawaiian region will be performed. Focus will then turn to a comparison between the mean seasonal climatology and those under trade wind conditions during summer and winter. The structure of the paper is as follows. In Section 2, the multi-year mean seasonal climatology of trade wind and non-trade wind conditions are presented. The data and methodology used for the study are described in Section 3. Section 4 presents the seasonal MBL height climatology as well as the climatology during trade wind only conditions; both derived from COSMIC RO refractivity measurements. Results during trade wind conditions are then compared with the seasonal MBL height climatology. Our analyses of the MBL heights over the open ocean will also be compared with those at the two Hawaii sounding sites. Finally, Section 5 contains the summary and conclusion.

2. Seasonal Climatology

Throughout the summer months of June, July, and August (JJA) the northeasterly surface flow is the most dominant flow regime and present approximately 90% of the time (Schroeder, 1993). Conversely, during the cool season (November-April) the wind pattern is not as uniform as its summer counterpart (Schroeder and Giambelluca, 1998). The pattern difference can be attributed to the annual migration of the NPSTH and polar jet stream, which leave the islands

vulnerable to Kona low pressure systems, upper level troughs, and cold fronts (Kodama and Businger, 1998; Schroeder, 1993). As a result, the surface trade wind flow is present less than 50% of the time during the core winter months of December, January, and February (DJF) (Schroeder, 1993). The interaction between the islands and the prevailing weather patterns over the Pacific region add layers of complexity during DJF.

Fig. 1. Map of central North Pacific Ocean with the locations of Lihue and Hilo shown. The red box denotes the analysis region: 10°N-45°N; 125°W-175°W.

2.1. Sea Level Pressure and Surface Wind

The maximum surface pressure associated with the NPSTH during JJA is approximately 1024 hPa and located near 35°N, 150°W as seen in the six year mean (2007-2012) from the National Centers for Environmental Prediction (NCEP) Final (FNL) Operational Global Analysis (Fig. 2). During the DJF season, the center of the NPSTH (1022 hPa) is located in the vicinity of 30°N, 130°W, southeast of the JJA position (Fig. 2). The location and strength of the NPSTH governs the prevailing surface wind over the central North Pacific region; accordingly, the effects of island interactions vary by season. Climatologically, the surface winds are predominantly from the northeast during JJA with a maximum mean velocity of approximately 7.5 m s^{-1} in an area located south of the Island of Hawaii and bisected by the 15°N latitude line between 150°W and 165°W (Fig. 2). Note that while the mean minimum surface wind vectors are seen in the lee of the Hawaiian Islands, the wake circulations (Hafner and Xie, 2003; Smolarkiewicz et al., 1988; Yang and Chen, 2003) are not properly resolved by the NCEP-FNL analysis. As the NPSTH shifts southeastward during DJF, the surface winds upstream of Hawaii shift to a more easterly direction with slightly slower wind speed, which moves the area of maximum mean wind speed (7.5 m s^{-1}) to the south side of the Big Island and east to west across the entire analysis domain south of 20°N (Fig. 2).

Fig. 2. Seasonal mean climatology of (top row) mean sea level pressure (MSLP in hPa) and (bottom row) surface wind vectors for JJA (left) and DJF (right) with isotachs in 2.5 m s^{-1} increments, during 2007-2012 based on NCEP-FNL Operational Global Analysis.

3. Data and Methods

3.1. National Center for Environmental Prediction–Final (NCEP FNL) Analysis Data

Because the difference in MBL height during trade wind and non-trade wind conditions is the primary focus of this study, daily (00 Z and 12 Z) surface maps of mean sea level pressure (MSLP) from the NCEP FNL Operational Global Analysis are utilized to identify "trade wind days". The NCEP FNL data are resolved on a 1°x1° grid with 26 mandatory levels every six hours. The analysis data are obtained from the Computational and Information Systems Laboratory Research Data Archive (http://rda.ucar.edu/datasets/ds083.2). For the purposes of this study, the required synoptic conditions to be considered as "trade wind" flow are as follows.

- Surface flow from the NPSTH not influenced by Kona lows, tropical cyclones, cold fronts, or other synoptic disturbances.
- Any 24-hour period with a disturbance interrupting or enhancing the northeast flow was not considered a trade wind day.

Examples of typical trade wind and non-trade wind surface flow for both JJA and DJF are presented in Fig. 3. During trade wind days, northeasterly winds originating from the NPSTH dominate the surface flow across the central North Pacific Ocean. During the non-trade wind days, the synoptic disturbance for both summer and winter seasons led to a decrease or even an absence of NE surface winds. During the six-year period (2007-2012), trade wind days account for 87% of the total observation days during JJA and 47% during DJF.

Fig. 3. Examples of mean sea level pressure (MSLP in hPa) and surface wind vectors (isotachs in 2.5 m s^{-1} increments) during typical trade wind (left column) and non-trade wind (right column) days from NCEP-FNL Operational Global Analysis. Selected JJA cases are 00Z-24 June 2009 (top left) and 00Z-01 July 2009 (top right). The selected DJF cases are 00Z-04 December 2012 (bottom left) and 00Z-11 December 2008 (bottom right).

3.2. COSMIC GPS Radio Occultation Soundings

The primary data set used is COSMIC RO refractivity profiles obtained through the Taiwan Analysis Center (http://tacc.cwb.gov.tw/cdaac/). Six years of COSMIC RO profiles over the Hawaiian region from 2007 to 2012 were collected and binned into 5°x5° latitude/longitude grids. Each RO profile was flagged as either trade wind or non-trade wind based on the synoptic condition from the NCEP FNL analysis. The focus is the seasonal climatology of the MBL height for Northern Hemisphere spring (March-April-May, MAM); summer (June-July-August, JJA); fall (September-October-November, SON); and winter (December-January-February,

DJF). Additionally, the climatology of the MBL height under trade wind conditions in summer and winter seasons (JJA-TW and DJF-TW) for the years 2007 through 2012 is included in the analysis.

3.3. Using the Gradient Method to Detect Inversion Base Height from GPS RO Soundings

The microwave refractivity, N (N-units), in the neutral atmosphere (Smith and Weintraub, 1953) is a function of atmospheric pressure (P in hPa), temperature (T in K), and water vapor partial pressure (P_w in hPa), such that

$$N = a_1(P/T) + a_2(P_w/T^2), \quad (1)$$

where a_1= 77.6 (K hPa^{-1}) and a_2 = 3.73 x 10^5 (K^2 hPa^{-1}). The first term on the right-hand-side of Eq. (1) represents the dry term of the refractivity value while the second term accounts for the contribution of moisture (Bean and Dutton, 1966). The vertical refractivity gradient [Eq. (2)] is calculated by differentiating the microwave refractivity equation [Eq. (1)] with respect to height (Ao et al., 2012), where

$$N' = (a_1/T)\,P' - [a_1(P/T^2) + 2a_2\,(P_w/T^3)]T' + (a_2/T^2)P_w' \,. \quad (2)$$

In Eq. (2), N', P', T', and P_w' are the vertical gradients of refractivity, pressure, temperature, and water vapor pressure, respectively.

The simple gradient method was used to estimate the MBL height from the RO refractivity profiles, i.e., to identify the height of the minimum refractivity gradient as the MBL height (Ao et al., 2012; Xie et al., 2012). To avoid bias in the MBL height climatology, all RO soundings within the analysis region were quality-controlled before being included for derivation of the climatology (Table 1).

Table 1. Summary of constraints for inclusion of GPS RO vertical profile.

In this study, any sounding that did not penetrate within 500 m above the mean sea level was discarded (Ao et al., 2012; Guo et al., 2011; Xie et al., 2012). The minimum refractivity gradient is identified for each RO sounding between the lowest height (≤ 500 m) and 3.5 km above the surface. Previous studies used a maximum height threshold between 3.5 km and 6.0 km (Ao et al., 2012; Guo et al., 2011; Xie et al., 2012) to account for larger boundary layer height variation, especially over land. For a study region over the open ocean, the maximum height threshold does not affect the general results of the paper. Moreover, to allow for a more robust MBL detection, the minimum refractivity gradient was required to be less than -40 N-units km^{-1}. When an inversion is present, a sharp moisture gradient exists at the top of the MBL over the analysis region resulting in a minimum refractivity gradient with values that frequently range between -60 and -80 N-units km^{-1} (Ao et al., 2012). With the implementation of data constraints, the number of valid RO profiles was reduced by roughly 50% from those that were initially available. All valid RO profiles were used to construct the seasonal MBL height climatology and then the analysis was focused on trade wind only profiles for JJA and DJF, based on the synoptic condition from the NCEP-FNL reanalysis. The zonal distribution of GPS RO observations (Fig. 4) shows a rather homogeneous sampling pattern between 10°N and 20°N; variability increases north of the island chain with a maximum located in the area of 30°N between 120°W and 140°W.

Fig. 4. Six year mean COSMIC RO sounding numbers per 5° x 5° grid in four seasons: DJF (top left); MAM (top right); JJA (bottom left); and SON (bottom right).

COSMIC sounding numbers under trade wind conditions (Fig. 5) do not vary during JJA-TW due to the large percentage (87%) of trade wind days in the summer season. Conversely, RO soundings under trade wind condition during DJF-TW reduced by about half as a result of a much smaller percentage (47%) trade wind days due to the much closer proximity at which synoptic disturbances pass the islands.

Fig. 5. Six year mean COSMIC RO sounding numbers per 5° x 5° grid under trade wind conditions for JJA-TW (left) and DJF-TW (right).

The simple gradient method was applied to each refractivity profile to calculate the minimum gradient value and associated height at which it occurs. The height of the minimum

refractivity gradient ($N' < -40$ N-units km^{-1}) defines the top of the MBL. Note that radiosonde observations indicate that the inversion base height is slightly lower but very consistent with the height of the maximum temperature gradient (de Szoeke et al., 2009). In this study, the minimum gradient heights derived from the RO refractivity sounding were used to represent the height of the MBL. After all the profiles were binned into 5° x 5° grids in the study region, median and standard deviation values for MBL height climatology were calculated.

3.4. Relative Minimum Gradient (RMG)

The relative minimum gradient (RMG) is a unitless value that quantifies the magnitude of the minimum refractivity gradient used to identify the top of the MBL (Ao et al., 2012). As seen in Eq. (3), the RMG (N'_{rmg}) is calculated by dividing the minimum refractivity gradient (N'_{min}) by the root mean square (RMS) of the refractivity gradient (N'_{rms}) [Eq. (4)] over the specified layer of the profile (between 500 m and 3.5 km). The resulting ratio provides a proxy to the strength of the gradient by comparing it to the RMS of the gradients within the layer. A RMG value of 1.0 means the minimum gradient is theoretically no different than the gradient values above or below that height. A sharp inversion layer is defined by a RMG value approaching twice the value of the layer mean RMG for this region.

$$N'_{rmg} = -(N'_{min}/N'_{rms}) \quad (3)$$

$$N'_{rms} = \sqrt{1/n(N_1'^2 + N_2'^2 + \cdots + N_n'^2)} \quad (4)$$

The typical structure of the trade wind inversion over the central North Pacific region features the strongest subsidence adjacent to the western coast of North America. The strength of the inversion decreases toward the west and south due to the increasing distance from the center of the NPSTH as well as increasing sea surface temperatures. The results show that the inversion strength, represented by RMG, is strongest adjacent to the California coast and weakens to the west toward the Hawaiian Islands and south toward the intertropical convergence zone (ITCZ).

4. Results

4.1 Seasonal Climatology of MBL Height

Figure 6 shows the distinct seasonal variation of the MBL height climatology based on six-years (2007-2012) of COSMIC RO refractivity profiles. The climatology in all seasons

features an increase of MBL height from a local minimum (< 1 km) near the coast of Southern California, southwestward to a much deeper MBL (~2km) centered near the Hawaiian Islands. The climatology is consistent with the decrease in large-scale, free tropospheric subsidence from a maximum over the cool eastern Pacific near the Southern California coast to the much warmer region around Hawaii (e.g., Riehl, 1979). The winter season (DJF) shows the largest difference when compared to the other seasons featuring a spread of both the centers of minimum and maximum MBL heights to larger regions. When comparing the MBL height during each season, the highest MBL median values are southwest of the island chain during MAM and appear to progress in a northeasterly direction through JJA until the high median value area of 2.0 km is centered directly over the islands during SON. DJF shows a lower MBL median value of 1.8 km to the south of the Big Island and to the west along the 15°N parallel. The seasonal variation of the median MBL values is consistent with those determined by the Hilo and Lihue soundings, which also show higher MBL during the spring and autumn seasons. However, the MBL inversion height climatology determined by two radiosonde sounding sites (Lihue and Hilo) in Hawaii shows the median values of MBL at Hilo are about 200 m higher than those at Lihue year round (Neiburger et al., 1961; Bingaman, 2005). In contrast, except for DJF during which the axis of the NPSTH is at its southernmost location (Fig. 3), the JJA median values of MBL determined by the GPS RO data are higher in the vicinity of Lihue than Hilo. Furthermore, the MBL median values determined by soundings, especially those from Hilo in JJA are higher than those determined by GPS RO data. It is apparent that the MBL heights on the windward side of the islands under trade wind conditions, especially the Hilo soundings, are affected by orographic lifting and will be discussed further in section 4.2.

The standard deviation (STDV) of MBL height in four seasons is shown in Figure 7. A minimum STDV value (~0.55 km) is seen over the subtropical latitude band (15°N-35°N) between Hawaii and California (120°W-150°W). In addition, a clear maximum STDV (over 0.7 km) is located west of the islands near (20°N, 165°W) in JJA and SON seasons.

The relative minimum gradient (RMG), a good proxy of the MBL inversion strength, is shown in Figure 8. The RMG shows the strongest gradient (> 2) near the coast of Southern California, which weakens southwestward with increasing distance from the NPSTH center (Fig. 2) and increased convective mixing when approaching the ITCZ. Near Hawaii, the inversion is strongest during the winter months (DJF). The primary reason for the higher RMG value during

SON and DJF can be explained by the southward shift of the ridge axis of the NPSTH toward the island chain (Fig. 2), which results in stronger subsidence and a lower MBL top. It is worth noting that the minimum STDV of the MBL height over the subtropical band (15°N-30°N, 120°W-150°W), is over the region of highest RMG values.

4.2. Characteristics of the MBL Height Climatology Under Trade Wind Conditions in JJA

The MBL climatology during JJA under trade wind only conditions (JJA-TW) is also derived based on the six-years of COSMIC RO refractivity profiles (Fig. 9). When compared with mean climatology of JJA (Fig. 6), the MBL height for JJA-TW over the entire island chain shows similar features; however the areal coverage of the deep MBL height (over 1.7 km) slightly increases under trade wind conditions (Fig. 9). In both the JJA and JJA-TW cases, the high median value of MBL height is located on the leeward side of the islands. West of Kauai (22.5°N, 162.5°W), the MBL height is approximately 2.1 km. It decreases from 2.0 km over Kauai to 1.9 km over the Big Island during JJA-TW, which is slightly lower than the typical inversion height determined by the Hilo soundings in JJA (~2.1 km) (Bingaman, 2005; Grindinger, 1992; Neiburger et al., 1961; Tran, 1995) on the windward coast of the Big Island (Fig. 1). It is apparent that the MBL height, as determined by the Hilo soundings, is not representative of the typical value for the Hawaiian Islands due to significant orographic lifting on the windward side of the Big Island caused by the presence of Mauna Loa and Mauna Kea, which have peaks well above the 4,000 m level (Smolarkiewicz et al., 1988; Yang and Chen, 2003).

The STDV of MBL height for JJA shows a minimum value of 0.55 km, which lies within the 15°N-35°N latitude band between the islands and California, and higher values of over 0.7 km located west of 165°W longitude (Fig. 7). Under trade wind conditions, the structure is similar; however, an increased area of the minimum STDV of 0.55 km is present (Fig. 9). Thus, under prevailing summer trade wind conditions, smaller variation of the MBL height covers a slightly larger area when compared to the mean climatology.

The bottom row of Figure 9 shows similar features of the RMG as the mean climatology shown in Figure 8, i.e., the strongest gradient is observed near the Southern California coast, which weakens to the south and west toward Hawaii. However, a significant increase in the area with relative strong gradients (RMG >1.5) under trade wind conditions is revealed.

4.3. Characteristics of the MBL Height Climatology Under Trade Wind Conditions in DJF

Throughout the DJF season, the mean MBL height climatology is lower under all conditions (Fig. 6) compared to trade wind (DJF-TW) conditions (Fig. 9). The majority of the island chain has median MBL height values between 1.7 and 1.8 km, with an estimated height over the Big Island between 1.8 and 1.9 km. The highest MBL height (1.9 km) in DJF-TW is centered near (15°N, 150°W) and covers an area much larger than that in the mean climatology. The STDV of MBL height estimates during DJF-TW are generally smaller than the mean climatology (Fig. 6) and the area with MBL height STDV of 0.55 km extends westward to cover the entire island chain and southward toward near 15°N (Fig. 9) under trade wind conditions. The magnitude of the RMG changes less between DJF and DJF-TW than the summer months (Figs. 8 and 9). The primary reason for this is the southward shift of the ridge axis as described in Section 4.1. Comparison of El Niño vs. non-El Niño MBL heights during DJF (not shown) agree with previous conclusions (Bingaman, 2005; Cao et al., 2007), which observe no appreciable difference between the two data sets. Bingaman (2005) noted that the winter drought in El Niño years (Lyons, 1982) is not related to lower MBL height in those years, rather, it is related to below normal rainfall from winter storms.

Fig. 6. Six year median value of the estimated MBL height (km) identified using the minimum refractivity gradient. The MBL height is taken as the median observation per 5° x 5° grid. DJF (top left), MAM (top right), JJA (bottom left), and SON (bottom right).

Fig. 7. Standard deviation of MBL median height (km) over the central North Pacific region. DJF (top left), MAM (top right), JJA (bottom left), and SON (bottom right).

Fig. 8. Horizontal distribution of inversion strength, estimated by the relative minimum gradient (RMG). The RMG is calculated per 5° x 5° grid, for DJF (top left), MAM (top right), JJA (bottom left), and SON (bottom right).

Fig. 9. Six year median value of the (top row) MBL height (km); (middle row) standard deviation of MBL height (km); and (bottom row) relative minimum gradient (RMG), per 5° x 5° grid under trade wind conditions for JJA-TW (left) and DJF-TW (right).

5. Conclusion

The island-scale climate and weather under trade wind conditions are not only related to the flow regime (Smolarkiewicz et al., 1988), but also the MBL height with the top identified as the base of TWI (Leopold, 1949, Chen and Feng 1995, 2001; Hartley and Chen 2013). Previous studies of the TWI (strength, height, seasonal variations) over Hawaii utilized rawinsonde data from two sounding sites (Lihue and Hilo), however, soundings taken at both sites are affected by terrain and local winds and may not represent the TWI over the open ocean. Routine observations of the MBL height over the coastal waters of Hawaii are lacking. The COSMIC GPS RO profiles with a vertical resolution as high as 100 m provide the opportunity to study spatial and seasonal variations of the height and strength of the MBL over the central North Pacific for the first time.

In this study our results show that during JJA, when the northeasterly trade winds are prevailing, the median MBL height decreases from 2.0 km over Kauai to 1.9 km over the Big Island with an approximate 2 km maximum that progresses from southwest of the region during MAM to a position directly over the Hawaiian Island chain during SON. If the surface flow is restricted to trade winds only for JJA and DJF, the maximum MBL heights are located over the same areas, but increase to 1.8 km and 2.1 km over the same area during the two respective time periods. The strength of the inversion is stronger when surface winds are restricted to trade wind flow only. In the composite JJA climatology, the relative minimum gradient (RMG) is below 2 over the island chain, however, under trade wind conditions the RMG factor over the majority of the islands is between 2.0 and 2.05. The typical MBL height (~ 2.2 km) from previous studies were determined by Hilo soundings (e.g., Schroeder 1993), which were taken on the windward coast of the Island of Hawaii and are probably affected by orographic lifting due to the peaks of Mauna Loa and Mauna Kea, which are well above the 4 km level (Garrett, 1980).

A different spatial pattern of the MBL height occurs during the winter months. During DJF, refractivity profiles reveal a stronger inversion as well as a lower inversion base height in

conjunction with the proximity of the NPSTH to the island chain. A high median MBL height of 1.8 km to the southeast of the Big Island increases to 1.9 km when the low level flow is restricted to trade wind flow. In part, this could be due to the seasonal shift of the NPSTH from north of the island chain during JJA to the southeast during DJF. Additionally, trade wind flow occurs only 47% of the time during DJF compared to 87% during JJA. The seasonal variability of MBL height could be the result of seasonal variations in large-scale circulation patterns causing increased variability in surface flow during the winter months. While the RMG factor reflects a value greater than 2.0 over the islands during trade wind conditions, the most noticeable difference occurs during the composite climatology analysis. The RMG factor over the island chain remains at a value of 2.0 or greater for the DJF composite, which is greater than the JJA composite value. The location of the ridge axis and proximity to the island chain during the winter season has resulted in lower MBL heights with stronger strengths than other seasons. The spatial distribution of the inversion height over Hawaii may be related to the horizontal distribution of large-scale subsidence as well as orographic effects of the island chain (Hafner and Xie, 2003). These issues will be investigated in the future using high resolution numerical models.

Acknowledgements

The authors would like to thank the anonymous reviewers for their valuable input on this research. COSMIC data were downloaded from the Taiwan Central Weather Bureau (http://tacc.cwb.gov.tw/cdaac/) whereas the NCEP-FNL data were downloaded from the Research Data Archive at the National Center for Atmospheric Research, Computational and Information Systems Laboratory, Boulder, CO [Available online at http://rda.ucar.edu/datasets/ds083.2]. Funding for this research was provided by the National Science Foundation award number AGS-1142558 to the University of Hawai'i at Mānoa. This project is also partially supported by NASA grant NNX14AK17G to Texas A&M University-Corpus Christi.

References

Albrecht, B.A., Betts, A.K., Schubert, W.H., and Cox, S.K., 1979. Model of the thermodynamic structure of the trade wind boundary layer: Part I. Theoretical formulation and sensitivity tests. *J. Atmos. Sci*., **36**, 73–89. doi:10.1175/1520-0469(1979)036<0073:MOTTSO>2.0.CO;2.

Ao, C.O., Waliser, D.E., Chan, S.K., Li, J.-L., Tian, B., Xie, F., and Mannucci, A.J., 2012. Planetary boundary layer heights from GPS radio occultation refractivity and humidity profiles. *J. Geophys. Res*., **117**, D16117. doi:10.1029/2012JD017598.

Basha, G., and Rantam, M.V., 2009. Identification of atmospheric boundary layer height over a tropical station using high-resolution radiosonde profiles: Comparison with GPS radio occultation measurements, *J. Geophys. Res*, **114**, D16101. doi:10.1029/2008JD011692.

Bean, B., and Dutton, E., 1966. *Radio Meteorology*. Dover Publications, 435 p.

Betts, A.K., and Ridgway, W., 1989. Climatic equilibrium of the atmospheric convective boundary layer over a tropical ocean. *J. Atmos. Sci*., **46**, 2621–2641. doi:10.1175/1520-0469(1989)046<2621:CEOTAC>2.0.CO;2.

Bingaman, J.B., 2005. Characteristics of the trade wind inversion over Hawaii. MS Thesis, Dept. of Meteorology, University of Hawaii at Mānoa, Honolulu, HI, 58 p. [Available from Dept. of Atmos. Sci. 2525 Correa Rd., Honolulu, HI 96822.]

Cao, G., Giambelluca, T.W., Stevens, D.E., and Schroeder, T.A., 2007. Inversion variability in the Hawaiian trade wind regime. *J. Climate*, **20**, 1145–1158.

Chen, Y.-L., and Nash, A.J., 1994. Diurnal variation of surface airflow and rainfall frequencies on the island of Hawaii. *Mon. Wea. Rev.*, **122**, 34–56.

Chen, Y.-L., and Wang, J.-J., 1994. Diurnal variation of surface thermodynamic fields on the island of Hawaii. *Mon. Wea. Rev.,* **122**, 2125–2138.

Chen, Y.-L., and Feng, J., 1995. The influences of inversion height on precipitation and airflow over the Island of Hawaii. *Mon. Weather Rev*., **123**, 1660–1676. doi: 10.1175/1520-0493(2001)129<1117:NSOAAC>2.0.CO;2.

Chen, Y.-L., and Feng, J., 2001. Numerical simulations of airflow and cloud distributions over the windward side of the Island of Hawaii. Part I: The effects of trade wind inversion*. *Mon. Weather Rev*., **129**, 1117–1134. doi:10.1175/1520-0493(2001)129<1117:NSOAAC>2.0.CO;2.

de Szoeke, S.P., Fairall, C.W., and Pezoa, S., 2009. Ship observations of the tropical Pacific Ocean along the coast of South America. *J. Climate*, **22**, 458–464. doi:10.1175/2008JCLI2555.1.

Garrett, A.J., 1980. Orographic cloud over the eastern slopes of Mauna Loa Volcano, Hawaii, related to insolation and wind. *Mon. Weather Rev*. **108**(7), 931–941. doi:10.1175/1520-0493(1980)108<0931:OCOTES>2.0.CO;2.

Giambelluca, T. W., Chen, Q., Frazier, A. G., Price, J. P., Chen, Y.-L., Chu, P.-S., Eischeid, J. K., and Delparte, D. M. 2013. Online rainfall atlas of Hawai'i. *Bull. Amer. Meteor. Soc.*, **94**, 313–316.

Grindinger, C.M., 1992. Temporal variability of the trade wind inversion measured with a boundary layer vertical profiler. M.S. Thesis, Dept. of Meteorology, University of Hawaii at Mānoa. 93 p. [Available from Dept. of Atmos. Sci. 2525 Correa Rd., Honolulu, HI 96822.]

Guo, P., Kuo, Y.-H., Sokolovskiy, S. V., and Lenschow, D.H., 2011. Estimating atmospheric boundary layer depth using COSMIC radio occultation data. *J. Atmos. Sci*., **68**, 1703–1713. doi:10.1175/2011JAS3612.1.

Hafner, J., and Xie, S.-P., 2003. Far-field simulation of the Hawaiian wake: Sea surface temperature and orographic effects*. *J. Atmos. Sci*., **60**, 3021–3032. doi:10.1175/1520-0469(2003)060<3021:FSOTHW>2.0.CO;2.

Hartley, T.M., and Chen, Y.-L., 2010. Characteristics of summer trade wind rainfall over Oahu. *Weather Forecast*., **25**, 1797–1815. doi:10.1175/2010WAF2222328.1.

Ho, S.-P., Peng, L., Anthes, R.A., Kuo, Y.-H., and Lin, H.-C., 2015: Marine boundary layer heights and their longitudinal, diurnal, and interseasonal variability in the southeastern Pacific using COSMIC, CALIOP, and radiosonde data. *J. Climate*, **28**, 2856–2872. doi: 10.1175/JCLI-D-14-00238.1.

Kodama, K.R., and Businger, S., 1998. Weather and forecasting challenges in the Pacific region of the National Weather Service. *Weather Forecast*., **13**, 523–546. doi:10.1175/1520-0434(1998)013<0523:WAFCIT>2.0.CO;2.

Leopold, L.B., 1949. The interaction of trade wind and sea breeze, Hawaii. *J. Meteorol*., **6**, 312–320. doi:10.1175/1520-0469(1949)006<0312:TIOTWA>2.0.CO;2.

Lyons, S.W., 1982. Empirical orthogonal function analysis of Hawaiian rainfall. *J. Appl. Meteorol*., **21**, 1713–1729.

Malkus, J.S., 1956. On the maintenance of the trade winds. *Tellus*, **8**(3), 335–350. doi: 10.1111/j.2153-3490.1956.tb01231.x.

Malkus, J. S. and H. Riehl, 1964. *Cloud Structure and Distributions over the Tropical Pacific Ocean*, University of California Press, Berkeley, 229 p.

Neiburger, M., Johnson, D., and Chien, C., 1961. The inversion over the eastern north Pacific Ocean. *Studies of the Structure of the Atmosphere over the Eastern Pacific in Summer*, Vol. 1, University of California Press, 94 p.

Nguyen, H.V., Y.-L. Chen, and F. Fujioka, 2010: Numerical simulations of island effects on airflow and weather during the summer over the Island of Oahu. *Mon. Wea. Rev*. **138**, 2253–2280.

Rasmussen, R.M., Smolarkiewicz, P., and Warner, J., 1989: On the dynamics of Hawaiian cloud bands: Comparison of model results with observations and island climatology. *J. Atmos. Sci.*, **46**, 1589–1608.

Riehl, H., 1979. *Climate and Weather in the Tropics*. Academic Press, London, 613 p.

Schroeder, T.A., 1993. Climate controls. In Sanderson, M. (Ed.), *Prevailing Trade Winds: Weather and Climate in Hawaii*, University of Hawaii Press, Honolulu, p. 126.

Schroeder, T.A., and Giambelluca, T., 1998. Climate. In Juvik, S.P., and Juvik, J.O. (Eds.), *Atlas of Hawaii*, University of Hawaii Press, Honolulu, p. 333.

Smith, E.K., and Weintraub, S., 1953. The constants in the equation for atmospheric refractive index at radio frequencies. *Proc. IRE*, **41**, 39–41. doi:10.1109/JRPROC.1953.274297.

Smolarkiewicz, P.K., Rasmussen, R.M., and Clark, T.L., 1988. On the dynamics of Hawaiian cloud bands: Island forcing. *J. Atmos. Sci*., **45**, 1872–1905. doi: 10.1175/1520-0469(1988)045<1872:OTDOHC>2.0.CO;2.

Tran, L.T., 1995. Relationship between the inversion and rainfall on the Island of Maui. M.S. Thesis, Dept. of Geography, University of Hawaii at Mānoa, 115 p. [Available from Dept. of Geography. 2424 Maile Way, Honolulu, HI 96822.]

Trenberth, K.E., and Stepaniak, D.P., 2003. Seamless poleward atmospheric energy transports and implications for the Hadley circulation. *J. Climate*, **16**, 3706–3722. doi: 10.1175/1520-0442(2003)016<3706:SPAETA>2.0.CO;2.

Xie, F., Wu, D.L., Ao, C.O., Mannucci, A.J., and Kursinski, E.R., 2012. Advances and limitations of atmospheric boundary layer observations with GPS occultation over southeast Pacific Ocean. *Atmos. Chem. Phys*., **12**, 903–918. doi:10.5194/acp-12-903-2012.

Yang, Y., and Chen, Y.-L., 2003. Circulations and rainfall on the lee side of the Island of Hawaii during HaRP*. *Mon. Weather Rev*., **131**, 2525–2542. doi: 10.1175/1520-0493(2003)131<2525:CAROTL>2.0.CO;2.

Zhou, C., and Chen,Y.-L. 2014. Assimilation of GPS RO and its impacts on simulations of trade wind inversion and a winter cold front. *Nat. Sci.*, **6**, 605–614. http://dx.doi.org/10.4236/ns.2014.68060.

Glossary of Terms

Climatology–the long term frequency and trend of conditions over a region or area.

COSMIC–Constellation Observing System for Meteorology, Ionosphere, and Climate.

GPS–Global Positioning .

Inversion–an increase in atmospheric temperature with height.

Marine boundary layer–the lowest part of the atmosphere that has direct contact with and is directly influenced by the surface of the ocean.

Radio Occultation–a remote sensing technique that can be used to measure the atmosphere of a planet by observing the behavior of a radio wave between two satellites as the planet passes between them.

Refractivity–a measure of the bending of a wave as it passes through a medium.

Trade wind–the prevailing surface winds found in the tropics. They are northeasterly in the northern hemisphere and southeasterly in the in summer hemisphere.

Trade wind inversion–A lower tropospheric temperature/moisture inversion that occurs in the tropics.

WRF–Weather Research and Forecasting model.

Figure 1 - Map of analysis region

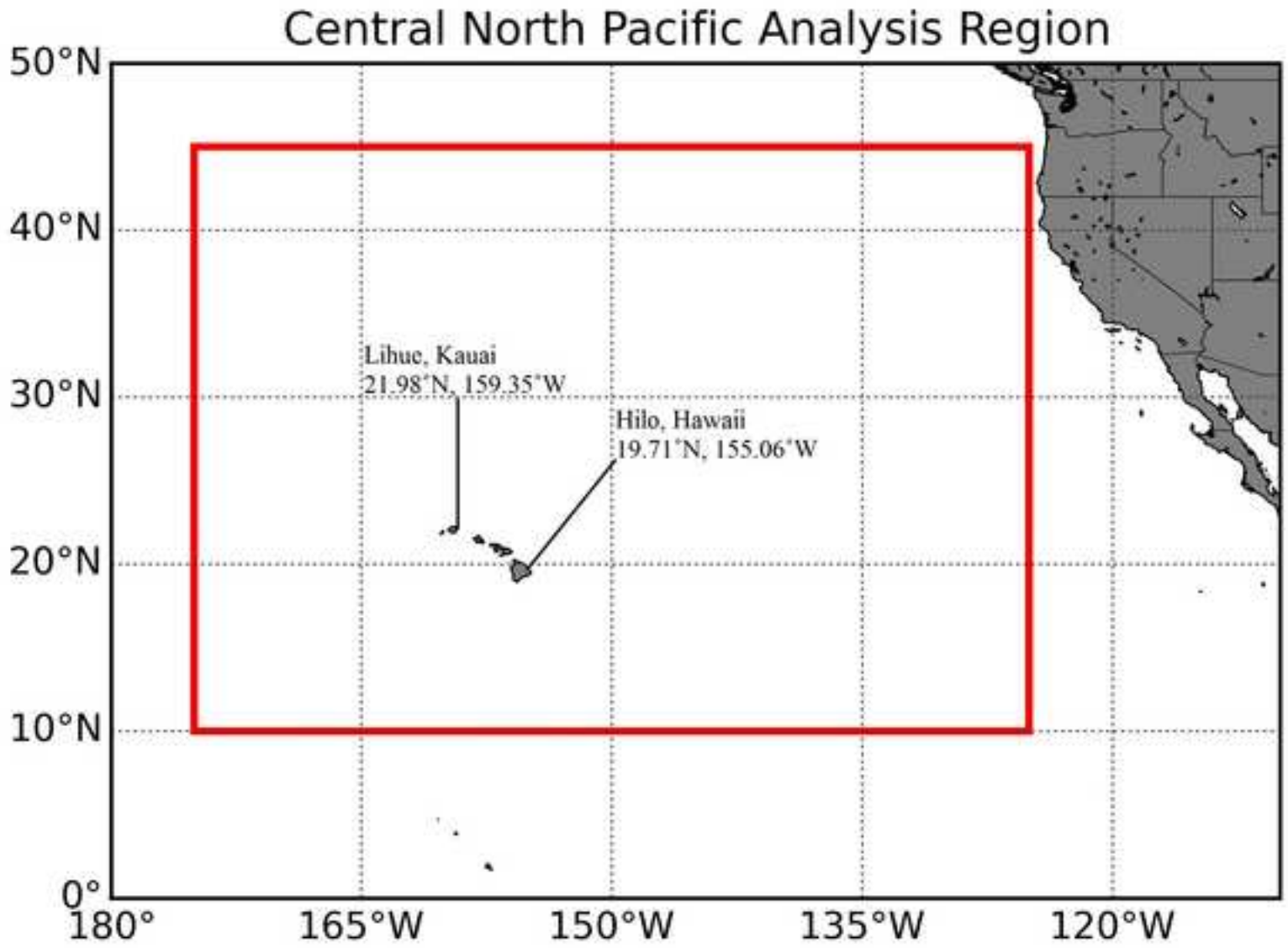

Figure 2

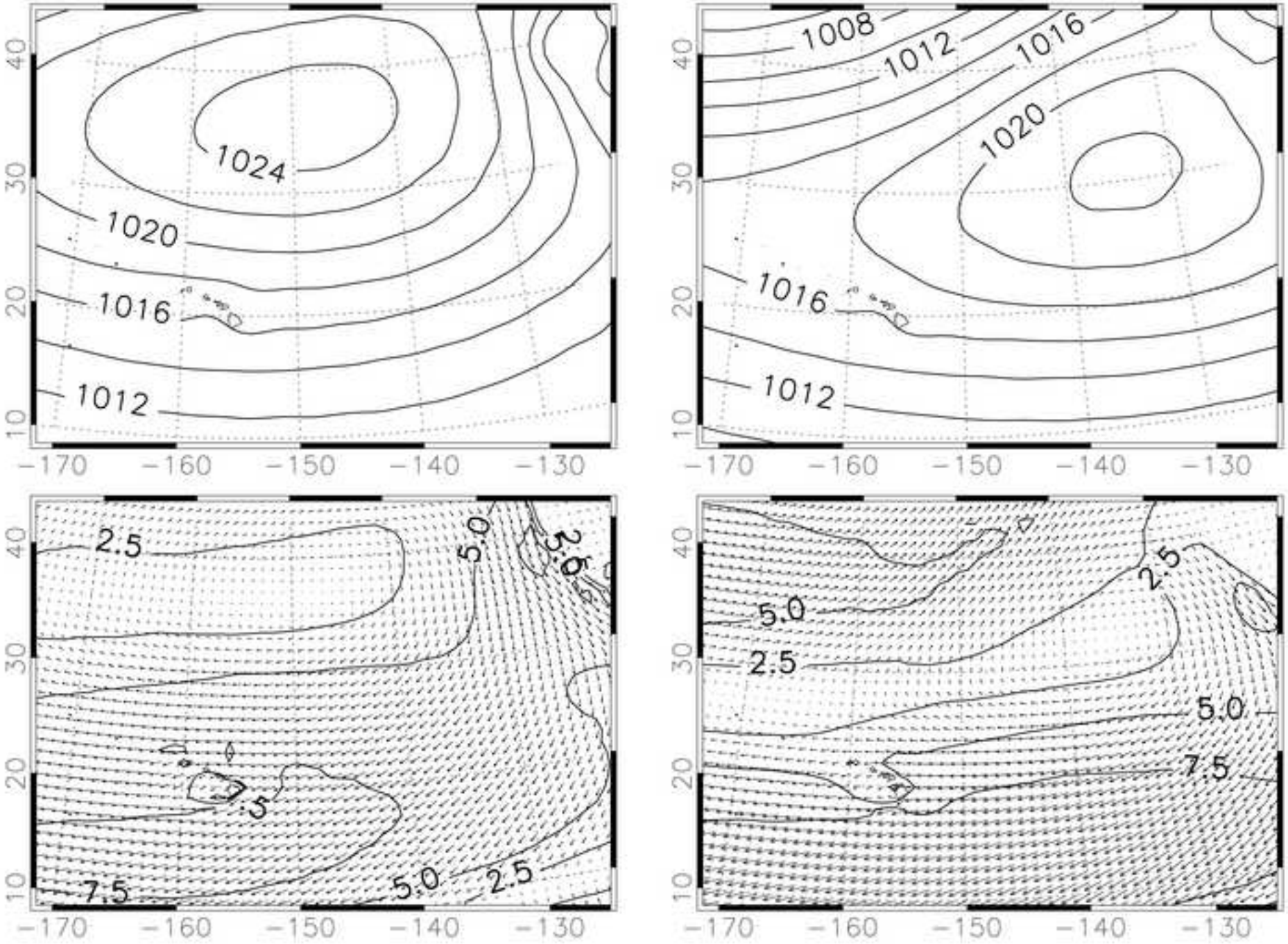
1024
1020
1016
1012
1008
1016
1020
1012
2.5
5.0
5.0
7.5
7.5
5.0
2.5
2.5
5.0
5.0
7.5
40
30
20
10
−170
−160
−150
−140
−130

Figure 3

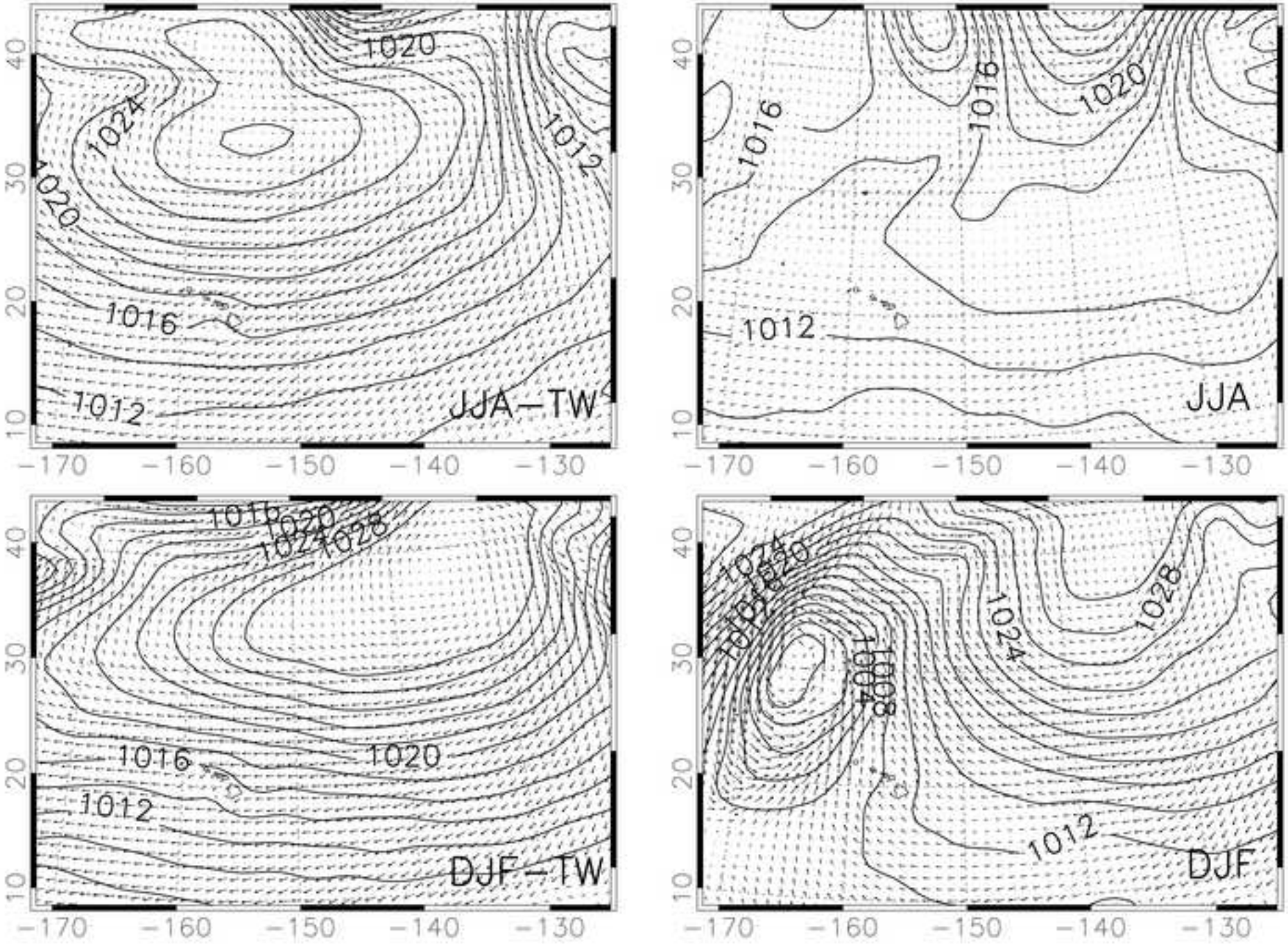
1020
1024
1020
1012
1016
1012
JJA–TW
1016
1016
1020
1012
JJA
1016
1020
1024
1028
1016
1020
1012
DJF–TW
1024
1020
1028
1024
1008
1004
1012
DJF
40
30
20
10
–170
–160
–150
–140
–130

Figure 4

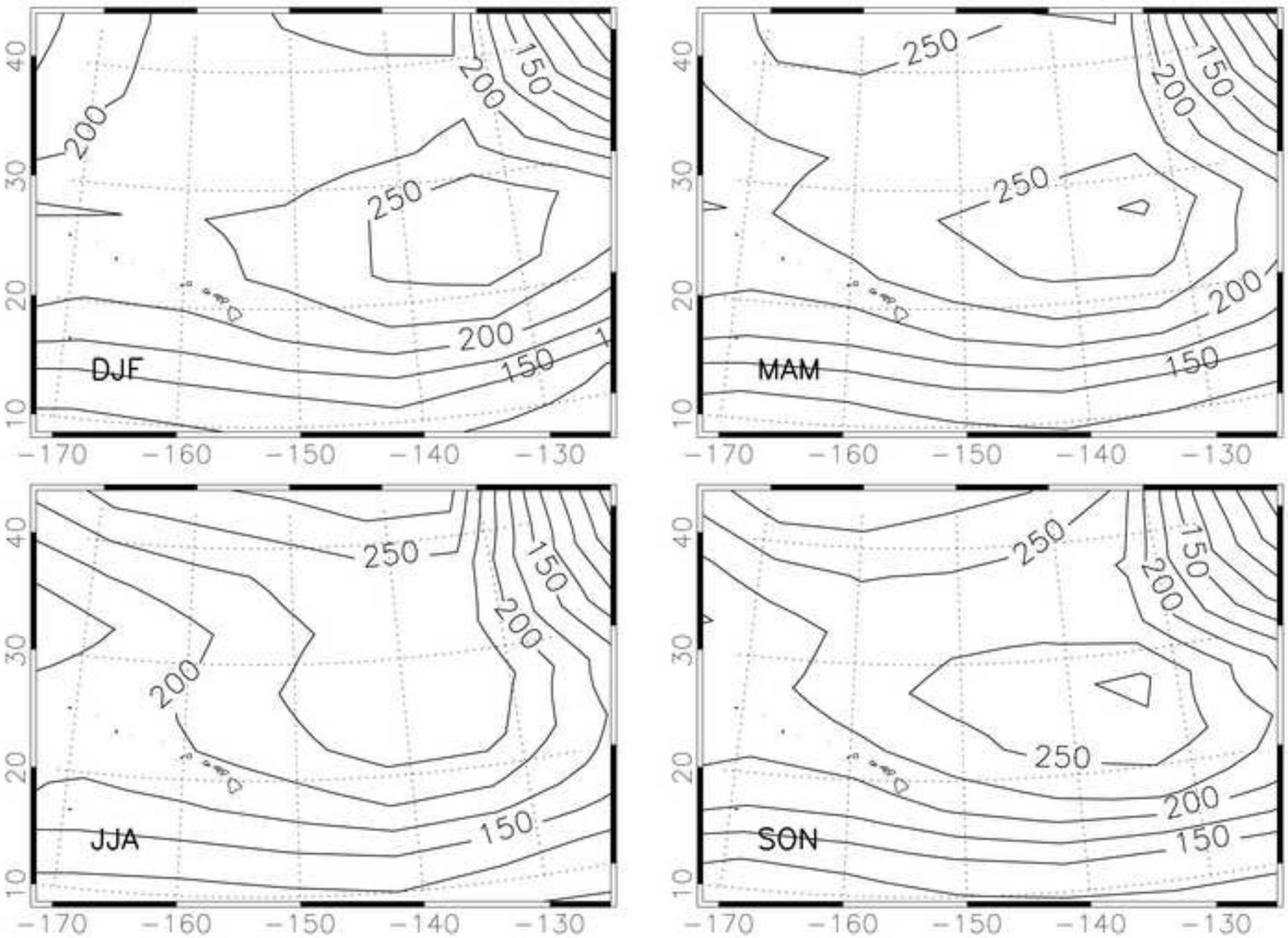

Figure 5

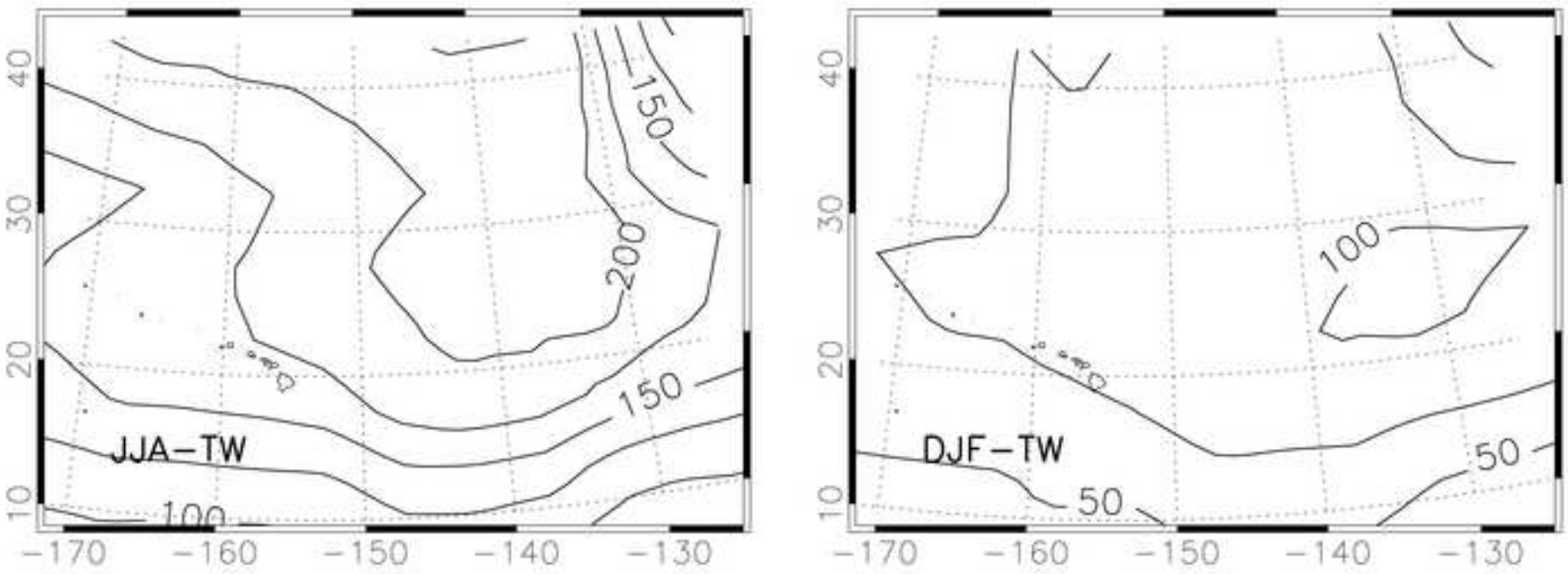
JJA−TW
150
200
150
100
DJF−TW
100
50
50
40
30
20
10
−170
−160
−150
−140
−130

Figure 6

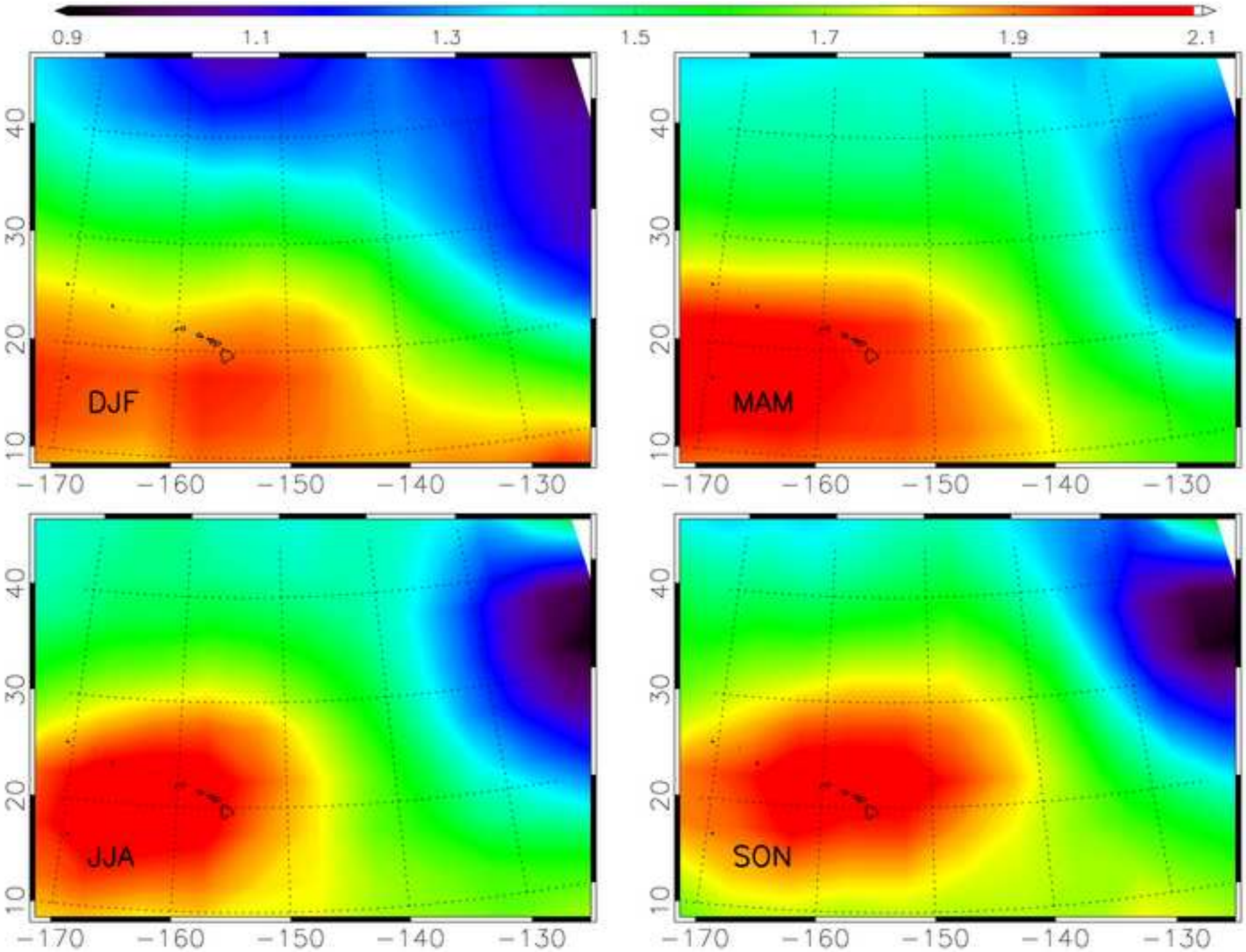

Figure 7

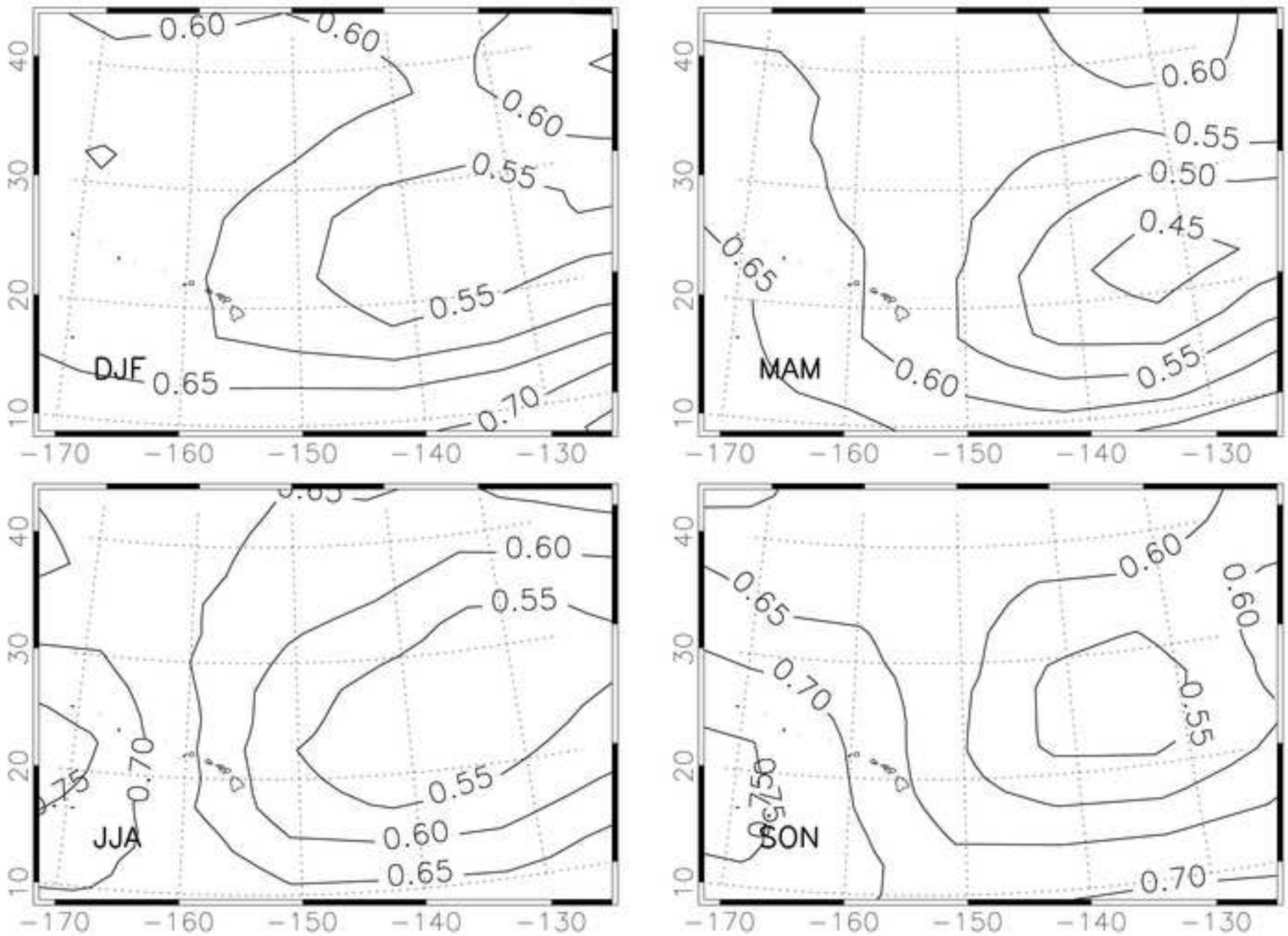
DJF
0.60
0.60
0.60
0.55
0.55
0.65
0.70
MAM
0.60
0.55
0.50
0.45
0.65
0.60
0.55
JJA
0.60
0.55
0.55
0.60
0.65
0.70
SON
0.60
0.60
0.65
0.70
0.55
0.70
40
30
20
10
−170
−160
−150
−140
−130

Figure 8

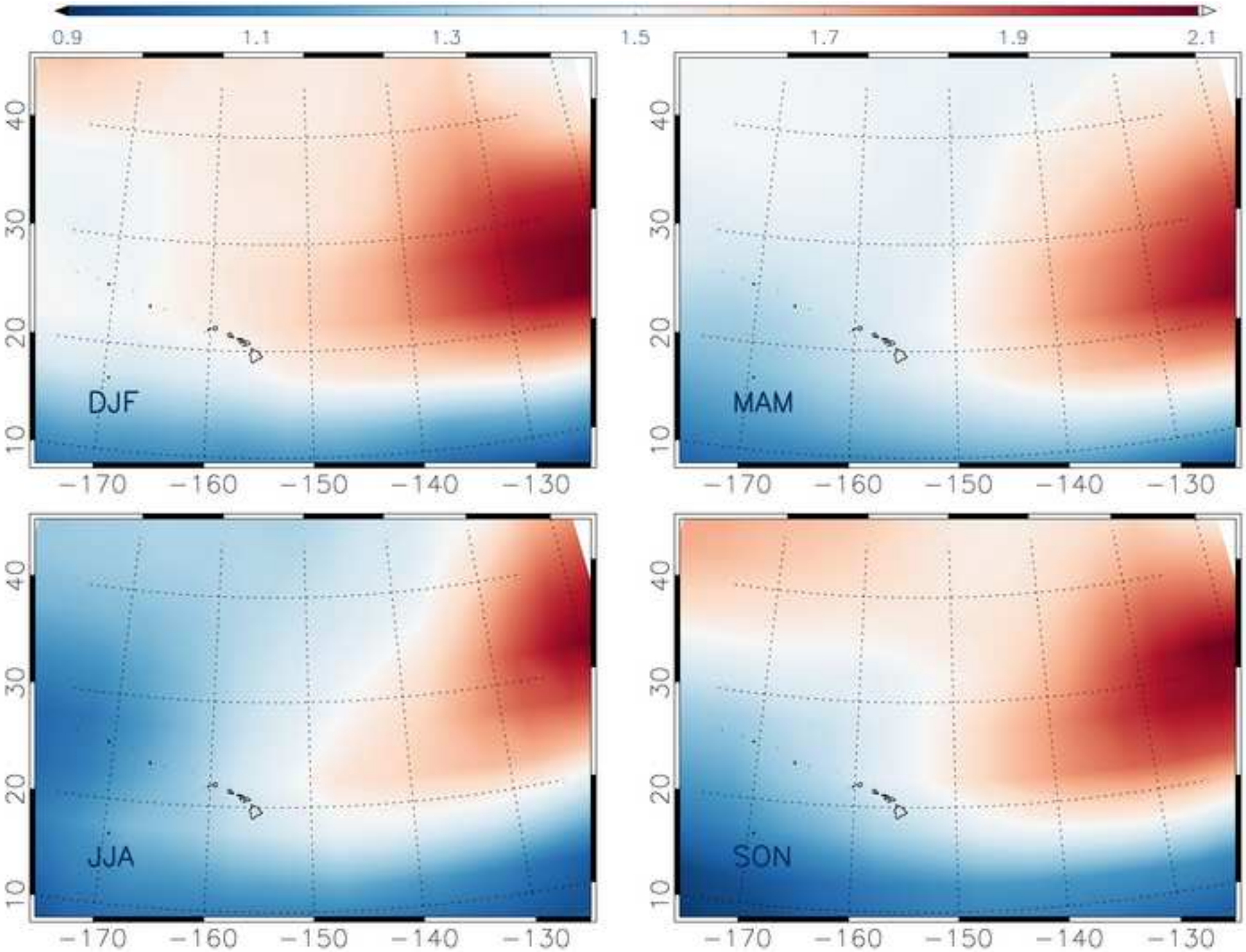

Figure 9 Top

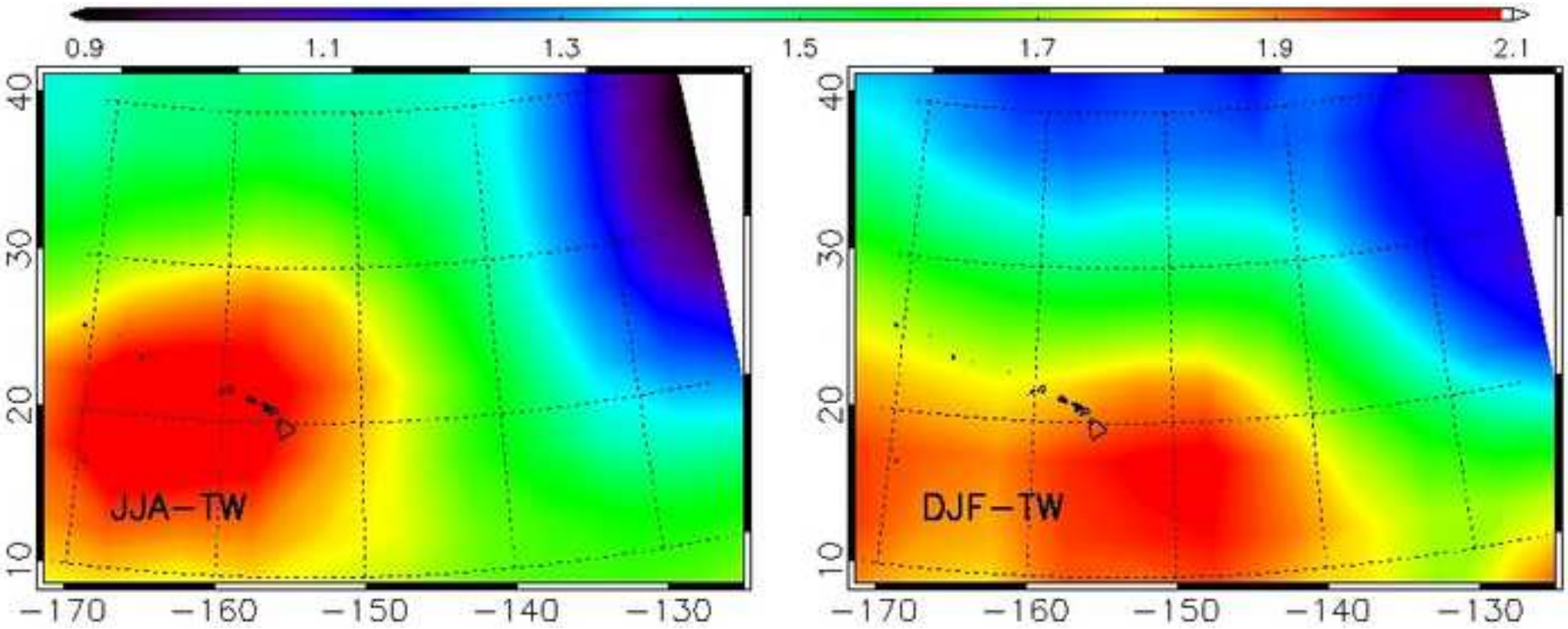

Figure 9 Middle

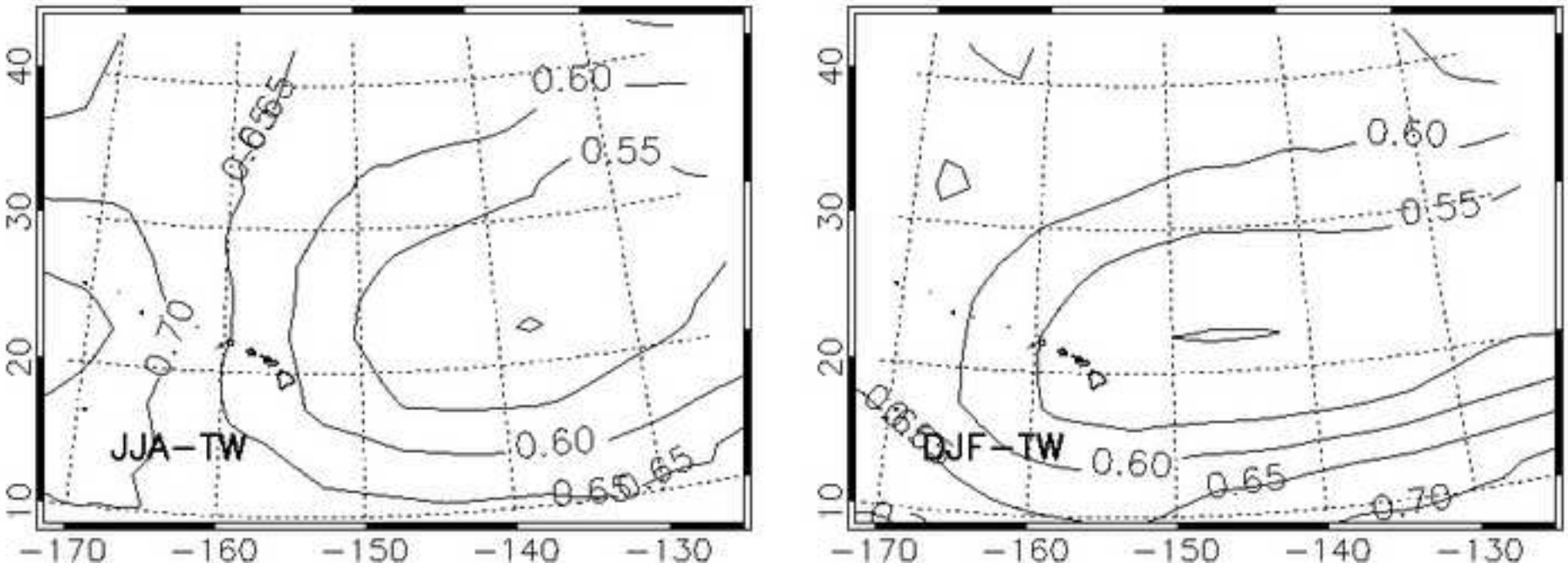

Figure 9 Bottom

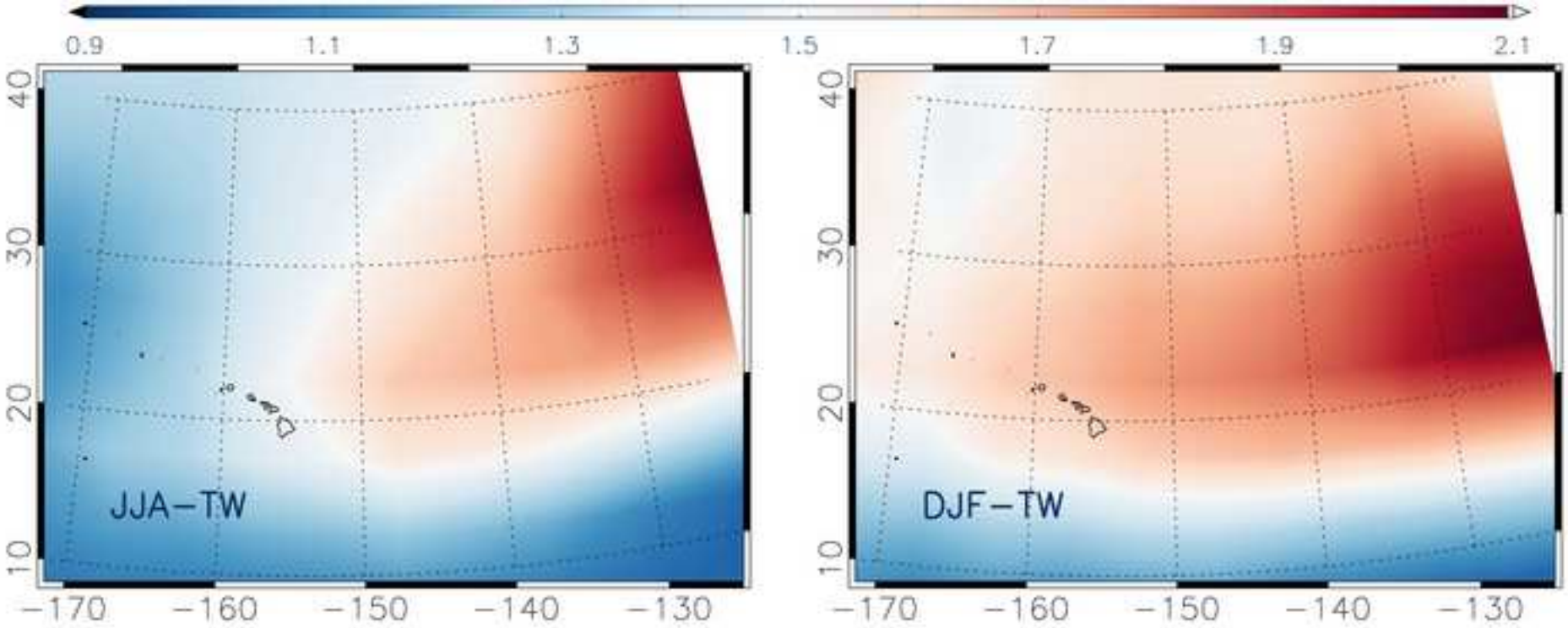

Table 1

Grid Bin Size	Minimum Height	Maximum Height	Minimum Refractivity Gradient
5° x 5°	≤ 500 m	≤ 3.5 km	< -40 N-units km^{-1}